Site selective 5f electronic correlations in β-uranium

Ruizhi Qiu(邱睿智)[1,†], Liuhua Xie(谢刘桦)[1,2], and Li Huang(黄理)[3,‡]

[1] *Institute of Materials, China Academy of Engineering Physics, Mianyang* 621907, *China*
[2] *School of Physical Science and Technology, Southwest University, Chongqing* 400715, *China*
[3] *Science and Technology on Surface Physics and Chemistry Laboratory, Mianyang* 621908, *China*

(Received 29 April 2022; revised manuscript received 31 May 2022; accepted manuscript online 8 June 2022)

We investigate the electronic structure of β-uranium, which has five nonequivalent atomic sites in its unit cell, by means of the density functional theory plus Hubbard-U correction with U from linear response calculation. It is found that the 5f electronic correlations in β-uranium are moderate. More interestingly, their strengths are site selective, depending on the local atomic environment of the present uranium atom. As a consequence, the occupation matrices and partial 5f density of states of β-uranium manifest site dependence. In addition, the complicate experimental structure of β-uranium could be well reproduced within this theoretical framework.

Keywords: uranium, low-symmetry crystal structure, 5f electronic correlation, site-selectivity, density-functional theory

PACS: 71.20.–b **DOI:** 10.1088/1674-1056/ac76ad

1. Introduction

Actinide metals exhibit a wide variety of exotic behaviors due to the complex nature of the 5f states.[1] At ambient pressure, some allotropes of light actinides exhibit quite complex crystal structures, in which the crystal symmetry is low and the number of atoms per unit cell is large. Three extreme cases are given by the α and β phases of plutonium (Pu) and β phase of uranium (U). Both α-Pu[2] and β-Pu[3] are monoclinic and there are 16 and 34 Pu atoms in the unit cell, respectively. For β-U,[4] the number of U atoms within the unit cell is as large as 30. These complex and low-symmetry crystal structures origin from the extremely narrow 5f band, which favors the Peierls distortion of the high symmetry lattice.[1,5]

The numbers of nonequivalent atoms in the unit cell of α-Pu, β-Pu, and γ-U are 8, 7, and 5, respectively. This implies that different actinide atoms in these phases probably have different amounts of electronic correlation. For α-Pu, the 5f electronic structures, including site-resolved density of states and hybridization functions, were investigated by means of a combination of density functional theory (DFT) and dynamical mean-field theory (DMFT).[6] It was argued that α-Pu's 5f electrons show apparent site dependence, which is interesting for a pure single-element material. Very recently, the same method (DFT + DMFT)[7] was employed to study the electronic structures of β-Pu.[8] The site-selective electronic correlations in β-Pu were confirmed, though its site selectivity is less prominent than that in α-Pu. The two pioneering works are quite important, but their conclusions are not solid. In their calculations, the same interaction parameters (Coulomb repulsion interaction U and Hund's exchange interaction $J_{\rm H}$) are adopted to describe the correlation effects on nonequivalent Pu atoms, which will introduce some sorts of non-consistency. In addition, the value of Coulomb interaction U used in these DFT + DMFT calculations is much larger than those from the first-principle evaluation of effective interaction.[9,10]

Here we concentrate on β-U, which is also an ideal playground for exploring how the electronic correlation varies with different sites. The determination of β-U structure is beset with difficulty because of lack of the single crystals of pure β-U. Thus, there is a controversy over the crystal structure of β-U during 1948–1974, although it was well-established that β-U is tetragonal with 30 atoms per unit cell.[11] Three suggested space groups are noncentrosymmetric $P4_2nm$ (No. 102), $P\bar{4}n2$ (No. 118) and centrosymmetric $P4_2/mnm$ (No. 136). The debate stems from the alloying elements and intrinsically complicate high-temperature x-ray powder diffraction. By using the advanced methods including neutrons and Rietveld profile, the controversy is resolved by Lawson and Olsen in 1988.[4] It was found that β-U has the centrosymmetric space group $P4_2/mnm$, as shown in Fig. 1. The 30 U atoms in the unit cell of β-U can be grouped into five nonequivalent types ($U_{\rm I}$, $U_{\rm II}$, $U_{\rm III}$, $U_{\rm IV}$, and $U_{\rm V}$). Their Wyckoff positions and atomic coordinates are collected in Table 1. Note that the space group of α-U structure ($Cmcm$) is also centrosymmetric and it is the subgroup of $P4_2/mnm$ rather than $P4_2nm$ and $P\bar{4}n2$. This crystal structure is also supported by the recent theoretical calculation.[12] Besides the structural properties, the elastic properties, electronic structures, and high-pressure behavior are investigated in the previous theoretical calculations.[12–14]

†Corresponding author. E-mail: qiuruizhi@caep.cn
‡Corresponding author. E-mail: huangli@caep.cn

© 2023 Chinese Physical Society and IOP Publishing Ltd

To the best of our knowledge, the 5f electronic correlations in β-U has not been well studied, the site-resolved electronic structure is unexplored, and the degree of freedom of 5f localization in this phase remains unknown.

In this work, the linear response approach[15] is used to determine the effective Coulomb interaction U for β-U and it is found that the values $U_{\rm LR}$ vary with different sites and are moderate. Our calculated results suggest that similar to α-Pu and β-Pu, β-U is another example that exhibits site selective 5f electronic correlations. Furthermore, the experimental lattice parameters of complex β-U could be well reproduced from the structural optimization within DFT$+U_{\rm LR}$.

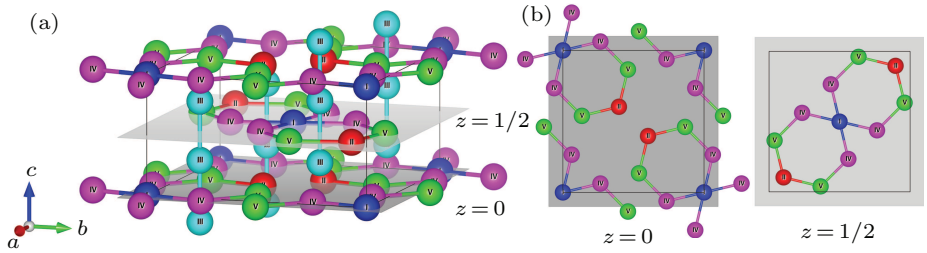


Fig. 1. (a) Schematic crystal structure of β-U. The uranium atoms at non-equivalent positions ($U_{\rm I}$, $U_{\rm II}$, $U_{\rm III}$, $U_{\rm IV}$, and $U_{\rm V}$) are represented by blue, red, cyan, purple, and green balls, respectively. The U–U bonds with bond length $d_{\rm U-U} < 3.0$ Å are visualized. (b) Schematic view of the $z = 0$ layer. (c) Schematic view of the $z = 1/2$ layer.

Table 1. The Wyckoff positions and atomic coordinates of β-U.[4]

sites	Wyckoff positions	x	y	z
$U_{\rm I}$	2a	0.0	0.0	0.0
$U_{\rm II}$	4g	0.3970	0.6030	0.0
$U_{\rm III}$	8j	0.3188	0.3188	0.2444
$U_{\rm IV}$	8i	0.0622	0.2657	0.0
$U_{\rm V}$	8i	0.1345	0.5391	0.0

2. Methods

Note that the DFT + DMFT method may be the most powerful approach ever established to study the electronic structures and physical properties of actinides.[7] It has been widely employed to study Pu and its compounds.[6,16,17] However, it requires huge computer resources and is extremely time-consuming. If there are multiple non-equivalent atoms in the unit cell, the situation becomes even worse. The reason is that each non-equivalent atom is described by a multi-orbital quantum impurity model, which should be solved by quantum impurity solvers repeatedly in the DMFT iterations. In the previous works about β-Pu, a simplified quantum impurity solver based on the one-crossing approximation was used,[8] with which the computational accuracy is restricted. In the present work, we adopt a traditional but more economic approach, namely DFT$+U$, to study the electronic structure of β-U.[18,19] Within this formalism, the structure optimization of complex β-U could be performed. This approach has been successfully applied to a large number of actinide metals and compounds.[10,20–24]

All the electronic structure calculations are performed using the Vienna *ab initio* simulation package (VASP).[25] The relativistic effect, i.e., spin–orbit coupling, is included in all the calculations. For the exchange-correlation term in the DFT Hamiltonian, the local-density approximation (LDA) of the Ceperley–Alder functional[26] and the generalized gradient approximation (GGA) of the Perdew–Burke–Ernzerhof (PBE) functional[27] are used. Although the interatomic distance is slightly larger, the fluctuation of the charge distribution in this bulk metallic system is not prominent enough to induce the dynamical correlation and thus the van der Waals interaction is not considered here. The Kohn–Sham equation is solved within the projector augmented wave formalism.[28,29] The valence electronic configuration for the U atom is $6s^2 6p^6 6d^1 5f^3 7s^2$. From the convergence tests, the optimal cutoff energy for plane wave basis is 450 eV and the division of Monkhorst–Pack k-mesh is $3\times3\times7$.

The 5f electronic correlations in U atoms are very important. We use a static mean-field scheme (i.e. the Hubbard-U correction method) to capture their contributions. According to the formalism of DFT$+U$, an on-site interaction term is added to the Hamiltonian, i.e.,[19]

$$E_U[\{\boldsymbol{n}^J\}] = \sum_J \frac{U^J}{2} {\rm Tr}\left[\boldsymbol{n}^J(1-\boldsymbol{n}^J)\right]. \tag{1}$$

Here J is the index of correlated atom, U^J is the effective Coulomb interaction, and $\boldsymbol{n}^J$ is the occupation matrix; $\boldsymbol{n}^J$ can be evaluated by the projection of Kohn–Sham orbitals ($\psi_{\boldsymbol{k},\nu}$) into the states of 5f localized orbitals (ϕ_m^J):

$$n^J_{mm'} = \sum_{\boldsymbol{k},\nu} f_{\boldsymbol{k},\nu} \left\langle \phi_m^J | \psi_{\boldsymbol{k},\nu} \right\rangle \left\langle \psi_{\boldsymbol{k},\nu} | \phi_{m'}^J \right\rangle, \tag{2}$$

where $\boldsymbol{k}$, ν, and m are Bloch wavevector, band index, and index of localized orbitals, respectively, and $f_{\boldsymbol{k},\nu}$ is the Fermi-Dirac distribution of the Kohn–Sham states.

For β-U, the values of effective interaction U^J for the five non-equivalent atoms is determined using the linear response approach (i.e., $U^J_{\rm LR}$).[10,15] The Hubbard parameter U^J could be evaluated as the second derivative of the ground state total energy with respect to the occupation number $n^J = {\rm Tr}[\boldsymbol{n}^J]$. The perturbed potential only acts on the localized orbitals of a Hubbard atom J, $\alpha^J|\phi_m^J\rangle\langle\phi_m^J|$ in which α^J is the amplitude. All occupation number $\{n^J\}$ vary in response to the change of

α^J and one can use this response function and the Legendre-Fenchel transformation to evaluate the Hubbard U^J. In numeric, an $1\times1\times2$ supercell is used and the response function is derived by setting α to ±0.1, ±0.2, ±0.3, ±0.4, ±0.5 eV.

The occupation matrix $\boldsymbol{n}^J$ is Hermite and the eigenvalues of this matrix could be denoted as $\{\bar{n}^J_m\}$, which could be used to determine the degree of 5f electronic localization or delocalization. In terms of $\{\bar{n}^J_m\}$, the Hubbard-U functional in equation (1) could be transformed as $\sum_{J,m}U^J\bar{n}^J_m(1-\bar{n}^J_m)/2$. Clearly, the fully localized electrons ($\bar{n}^J_m\sim1$) and empty occupation ($\bar{n}^J_m\sim0$) are energetically favorable. Thus, the Hubbard-U correction scheme favors Mott localization (i.e., insulating feature), instead of fractional occupation of localized orbitals (i.e., the metallic-like hybridization). We can use the following quantity to measure the degree of 5f delocalization for each correlated atom:

$$\mathcal{D}^J=\sum_m\bar{n}^J_m(1-\bar{n}^J_m). \tag{3}$$

If the 5f electrons tend to be fully localized, $\bar{n}^J_m\sim1$ or 0 and $\mathcal{D}^J\sim0$. On the contrary, if the 5f electrons favor itinerant states, $\bar{n}^J_m$ is far away from 1.0 and $\mathcal{D}^J$ is much greater than 0.

In the practical DFT+U calculations, electronic metastable states often emerge.[23] For the system with various interaction parameters, the problem is much worse. To circumvent this problem, we employ the U-ramping scheme[30] with increment in steps of 0.05 eV. Some quantities such as $\mathcal{D}^J$ could be shown as a function of the effective interaction U. For other physical quantities, we consider five different cases: $U=U_{\rm LR}$, 0.0 eV, 1.0 eV, 2.0 eV, 2.5 eV.

3. Results and discussion

3.1. Perspective from atomic structure

Let us first pay close attention to the atomic structure of β-U. As is shown in Fig. 1(a), the lattice of β-U is tetragonal and centrosymmetric. There are two planar atomic configurations in the $z=0$ [Fig. 1(b)] and $z=1/2$ [Fig. 1(c)] layers of the unit cell. According to the space group of β-U (No. 136), these two layers are equivalent and could be transformed to each other by using the rotation of 90° along c axis and translation of $(1/2,1/2,0)$. In the atomic layer, the configuration consists of U_I, U_{II}, U_{IV}, and U_V atoms and they form two connected hexagons. Note that the hexagons are not regular. The connected points of the two hexagons are occupied by the U_I atom. The four neighbor positions of connected points are occupied by U_{IV} atoms, and the U_V atoms occupy the four extended positions. The two terminal vertices of the two connected hexagons are occupied by U_{II} atoms. Besides the planar configurations, the residual U_{III} atoms constitute the bars which intersect the hexagons.

The calculated distribution of neighbors for each nonequivalent atoms are illustrated in Fig. 2. Here only the U–U interatomic distances up to 3.6 Å were taken into account. Note that there are no bonds with bond length ranging from 3.15 Å to 3.22 Å, as indicated by the dashed lines in Fig. 2. Thus we could classify the bonds in a similar way to β-Pu.[3,8] One group of short bonds with length ranging from 2.6 Å to 3.15 Å and the other group of long bonds with length ranging from 3.22 Å to 3.6 Å are defined. Within this classification, the number of bonds and the corresponding average bond lengths for each U site are computed, as listed in Table 2.

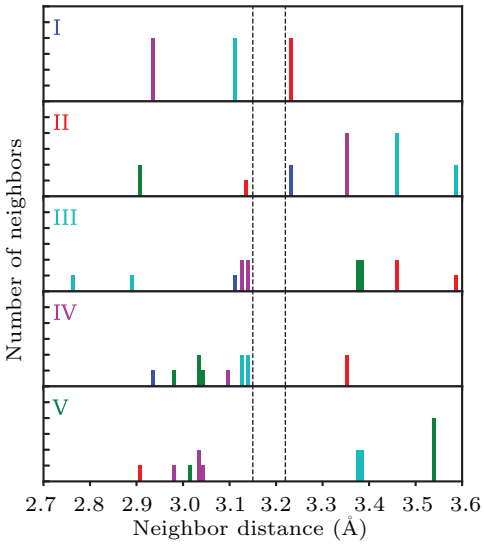


Fig. 2. Distribution of neighbors for each U site in β-U. The height of the bar means the number of neighbors and the color represents the bonding nonequivalent atom. The nonequivalent atoms U_I, U_{II}, U_{III}, U_{IV}, and U_V are represented by blue, red, cyan, purple, and green bars, respectively. Note that the U_V–U_V bond around 3.01 Å was absent in Ref. [4]. Two groups of bonds, i.e., short and long bonds, are separated by the dashed line.

Table 2. The number of short and long bond lengths in β-U. Here, $U_{\rm LR}$ denotes the Coulomb interaction parameter obtained from the linear response approach. See the main text for more details. Note that this experimental structure is different from the structure used in our previous calculation,[10,31] which is obtained from Pearson's Handbook.[32]

Sites	Short	$\bar{d}_{\rm short}$ (Å)	Long	$\bar{d}_{\rm long}$	$U_{\rm LR}$ (eV)
U_I	8	3.02	4	3.23	2.5
U_{II}	3	2.98	12	3.41	2.7
U_{III}	7	3.04	7	3.43	2.5
U_{IV}	10	3.07	2	3.35	2.5
U_V	6	3.00	8	3.46	2.6

Note that the number of short bonds for $U_{I,III,IV}$ is large, which implies that these sites may be relatively clustered. In Fig. 2, one can find that the first and second nearest-neighbors of U_I are U_{IV} and U_{III}, respectively. In addition, U_{III} and U_{IV} are bonded to each other around 3.13 Å. In contrast, there is only three short bonds for U_{II} site. This means that the site U_{II} is relatively isolated. The intermediate case is U_V.

3.2. Site-resolved interaction parameters

Now we employ the linear response approach to determine the interaction parameters U^J for the five non-equivalent

U atoms.[10,15] The calculated results using the PBE exchange-correlation functional and $1 \times 1 \times 2$ supercell are also collected in Table 2. The other exchange–correlation functionals such as LDA[26] and the solid variation of the PBE functional (PBEsol) are also examined. The calculations are also performed using the conventional unit cell. All calculations yield the same results within the accuracy of 0.1 eV. These benchmark calculations suggest that our calculations are reliable and the dominant effect is indeed the local atomic environment.

From Table 2, one can find that the U_{II} atoms have the largest U_{LR} (= 2.7 eV), which means that their 5f electrons are more localized than the others. The $U_{I,III,IV}$ atoms have the smallest U_{LR} (= 2.5 eV), which means that their 5f electrons are more itinerant and more easily hybridized with conduction electrons than the others. The intermediate case of U_V has the intermediate value $U_{LR} = 2.6$ eV. These results also suggest that the interaction parameter has the similar sequence with the number of short bonds in Table 2. The categories as proposed above are confirmed.

Note that the range of calculated interaction parameters U^J, i.e., [2.5 eV, 2.7 eV], is small. As can be seen in the following, it is also appropriate to use a same value of Hubbard U, such as 2.5 eV, for the DFT + U calculations. However, it is physically consistent to use different interaction parameters for different sites since it results from different local atomic environments. In addition, the difference of U among different nonequivalent sites is not small for the other low-symmetry structure, such as α-Pu and β-Pu.[10] In those cases, it is necessary to use different values of U for different nonequivalent sites.

3.3. Degree of delocalization

From the self-consistent DFT and DFT + U ($U = U_{LR}$, 1.0 eV, 2.0 eV, and 2.5 eV) calculation, the occupation matrices $\boldsymbol{n}^J$ and the corresponding eigenvalues $\bar{n}^J_{m=1,\ldots,14}$ for each nonequivalent atoms U_{I-V} are obtained. These eigenvalues are shown in Fig. 3. For DFT and DFT + U with $U = 1.0$ eV, the site dependence of $\bar{n}^J_m$ is not obvious. All the values of $\bar{n}^J_m$ are small and approximately uniform, which implies that all the 5f electrons are delocalized. In contrast, the profile of eigenvalues manifests its site dependence for DFT + U with $U = 2.0$ eV. There is one large eigenvalue in the cases of U_{IV} and U_V and two relatively large eigenvalues for U_{II}. For U_I and U_{III}, the values of $\bar{n}^J_m$ are still close to uniform. This indicates that the Hubbard interaction gradually induces the localization of 5f electrons for $U_{II,IV,V}$. For larger value of U, i.e., $U = 2.5$ eV, the Hubbard interaction driven localization of 5f electrons is more obvious. For U_{II}, all the eigenvalues are approximately equal to 1 or 0. The 5f localization in this site is evident. The site dependence of 5f delocalization could also be found within DFT + U with $U = 2.5$ eV. As comparison, the two largest eigenvalues for U_I are smaller than those for U_{II}. In particular, the site-dependent Hubbard U^J_{LR} results in huge differences for each nonequivalent site. From the profile of eigenvalues in the last row of Fig. 3, it is clear that the 5f electrons of U_I and U_{II} are delocalized and localized, respectively. In addition, the two 5f electrons around U_{IV} and U_V become localized in this case.

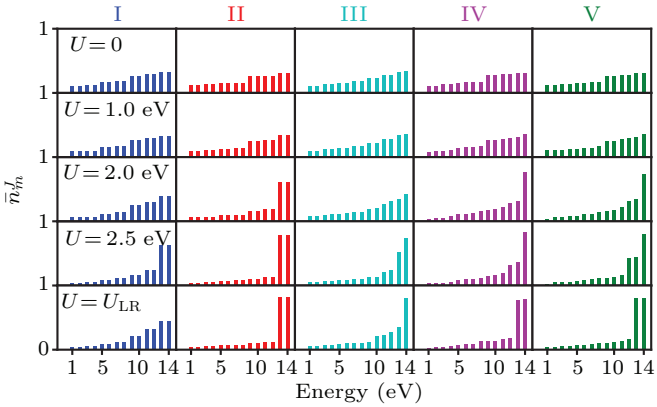


Fig. 3. The eigenvalues of occupation matrix $\bar{n}^J_m$ for the five nonequivalent U atoms (from left to right) of β-U obtained by DFT + U calculations. The nonequivalent atoms U_I, U_{II}, U_{III}, U_{IV}, and U_V are represented by blue, red, cyan, purple, and green bars, respectively. Here five different cases are considered. They are U = 0.0 eV, 1.0 eV, 2.0 eV, 2.5 eV, and U_{LR} (from top to bottom).

Table 3. The degree of delocalization $\mathcal{D}$ (3) for U_{I-V} within DFT + U calculations. Here we considered five cases: U = 0.0 eV, 1.0 eV, 2.0 eV, 2.5 eV, U_{LR}. Note that the order of $\mathcal{D}$ is same as that of $\bar{n}_m$ in Fig. 3.

	U_I	U_{II}	U_{III}	U_{IV}	U_V
U = 0 eV	2.17	2.11	2.17	2.17	2.16
U = 1.0 eV	2.09	2.03	2.09	2.08	2.07
U = 2.0 eV	1.94	1.64	1.98	1.70	1.71
U = 2.5 eV	1.64	1.23	1.60	1.54	1.49
$U = U_{LR}$	1.84	1.13	1.59	1.32	1.22

Using the definition of the degree of delocalization $\mathcal{D}$ (3), one can quantitatively describe the dependence of localization with respect to atomic site and Hubbard U. Table 3 presents the values of $\mathcal{D}$ for the five nonequivalent atoms and DFT + U calculation with $U = 0.0$ eV, 1.0 eV, 2.0 eV, 2.5 eV, and U_{LR}. The value of $\mathcal{D}$ decreases with the increasing U, which confirms the Hubbard interaction driven localization of 5f electrons. In addition, the differences of $\mathcal{D}$ among the five nonequivalent sites are very slightly different for DFT and DFT + $U = 1.0$ eV, but prominent for DFT + U with larger U. For DFT + U with $U = U_{LR}$, the value of $\mathcal{D}$ for U_{II} is the smallest and that for U_I is the largest. This means that the 5f electrons of U_{II} are the most localized and those of U_I are the most delocalized. For all DFT + U calculations, the degree of delocalization has the same sequence:

$$\mathrm{I} \gtrapprox \mathrm{III} > \mathrm{IV} > \mathrm{V} > \mathrm{II}. \tag{4}$$

Here the approximation in $\gtrapprox$ only applies to the case of $U = 2.0$ eV. As discussed above, the few short bonds for U_{II} results in the isolated local atomic environment and then the strong 5f electronic localization. Many short bonds for U_I

yield a clustered environment and then the 5f delocalization. The sequence of $\mathcal{D}$ is approximately same as that of numbers of short bonds except U_{IV}, in which the average short bond length is largest. This site dependence of $\mathcal{D}$ illustrates the site dependence of 5f delocalization, i.e., the site selective electronic correlations in β-U.

3.4. The 5f partial density of states

In Fig. 4, the calculated 5f partial density of states (pDOS) for the five non-equivalent U atoms are shown. Both DFT and DFT + U ($U^J = U_{LR}$, 1.0 eV, 2.0 eV, and 2.5 eV) are considered. For DFT or DFT + U = 1.0 eV, the differences of spectra among $U_{I–V}$ sites are inapparent. The main peaks of pDOS situate above the Fermi level. There are more small peaks with lower intensities below the Fermi level. The appearance of the multi-peak feature indicates that there is a strong hybridization between 5f and other conduction electrons. In addition, the increase of pDOS towards the Fermi level is approximately monotonous.

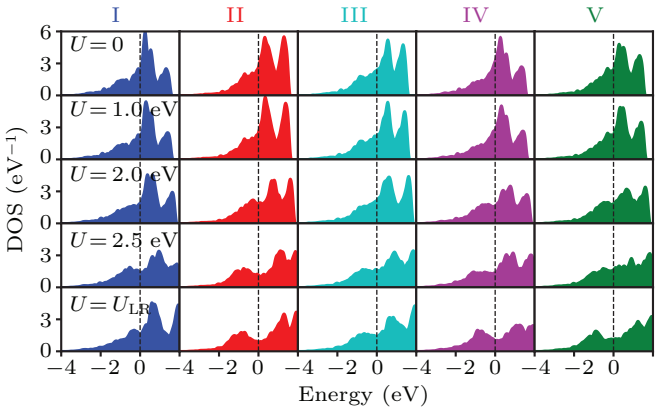


Fig. 4. The 5f partial electronic density of states for the five non-equivalent U atoms (from left to right) of β-U obtained by DFT + U calculations. The vertical dashed line denotes the Fermi level. The nonequivalent atoms U_I, U_{II}, U_{III}, U_{IV}, and U_V are represented with blue, red, cyan, purple, and green bars, respectively. Here, five different cases are considered. They are U = 0.0 eV, 1.0 eV, 2.0 eV, 2.5 eV, and U_{LR} (from top to bottom).

In contrast, a large peak appears below the Fermi level for DFT + U with larger U. This is the consequence of Hubbard interaction, and the peak corresponds to the so-called lower Hubbard bands. When U is increased, the Hubbard bands are pushed away from the Fermi level, and the spectral weights near the Fermi level are reduced. The site dependence of pDOS also manifests itself here.

From the profile of pDOS in the last row of Fig. 4 from DFT + U_{LR}, while the Hubbard peak is far from the Fermi level for U_{II}, it is still close to the Fermi level for U_I. This is a remarkable feature of the 5f electron localization for U_{II}. For U_I, the Hubbard bands are shifted below the Fermi level slightly. The distance of Hubbard peak from the Fermi level is closely related to the 5f electronic localization. Clearly, the 5f electrons of U_{II} is much localized than that of U_I. From the pDOS profile, the degree of localization for $U_{IV,V}$ is close to that for U_{II} while the degree of localization for U_{III} is close to that for U_I. This is consistent with the sequence of $\mathcal{D}$ (4).

3.5. Structural property

For β-U, the structural properties were already well described by GGA calculations.[12–14] This is confirmed by our PBE calculation of lattice parameters, as shown in Table 4. Table 4 also shows the calculated lattice parameters from LDA, LDA + U with U = 2.5 eV and U_{LR} calculations. One can find that the lattice constants are underestimated by LDA due to the over binding. This discrepancy could be remedied by the Hubbard correction. The lattice constants and the internal lattice parameters could be well reproduced by LDA + U = 2.5 eV and LDA + U_{LR} calculations. In particular, for the internal parameters z_{III} and x_{IV}, the PBE results deviate from the experimental data while LDA + U performs well. This improvement of DFT + U over PBE already found in the literature[10,24] is confirmed here, particularly for a complicate structure.

Table 4. Lattice parameters from experiment,[4] PBE, LDA, and LDA + U with U = 2.5 eV, and U_{LR} calculations. The percent in the bracket represent the error of calculated results from experimental data.

	exp.	PBE	LDA	LDA + U = 2.5 eV	LDA + U_{LR}
a	10.7589	10.4800	10.2346	10.9604	11.1453
		(–2%)	(–4%)	(1%)	(3%)
c	5.6531	5.6237	5.4796	5.7106	5.7205
		(0%)	(–3%)	(1%)	(1%)
x_{II}	0.3970	0.3915	0.3927	0.3989	0.3990
		(–1%)	(–1%)	(0%)	(0%)
x_{III}	0.3188	0.3206	0.3205	0.3187	0.3198
		(0%)	(0%)	(0%)	(0%)
z_{III}	0.2444	0.2288	0.2309	0.2439	0.2428
		(–6%)	(–5%)	(0%)	(0%)
x_{IV}	0.0622	0.0584	0.0578	0.0638	0.0634
		(–6%)	(–7%)	(2%)	(1%)
y_{IV}	0.2657	0.2652	0.2668	0.2610	0.2606
		(0%)	(0%)	(–1%)	(1%)
x_V	0.1345	0.1354	0.1361	0.1296	0.1298
		(0%)	(1%)	(–3%)	(–3%)
y_V	0.5391	0.5450	0.5461	0.5388	0.5379
		(1%)	(1%)	(0%)	(0%)

4. Conclusion

In summary, we have investigated the 5f electronic structures of β-uranium (β-U) using the DFT and DFT + U approaches. We determine the site-resolved interaction parameters, and confirm the existence of site-selective electronic correlation in β-U. For the atoms in the connect point of the two connected hexagons (i.e., U_I), the 5f electrons are highly delocalized. For the atoms in the terminal vertices of the hexagons (i.e., U_{II}), the 5f electrons are strongly correlated. The degree of localization on each position is closely related to the local atomic environment. This conclusion is supported by the analyses of the neighbor distance, the occupation matrix, and the 5f

partial density of states of β-U. Obviously, this site-selective electronic correlation may be a generic feature for those actinide metals which have multiple non-equivalent sites in the unit cell. Thus, we believe that the high-pressure phases of Am,[33] Cm,[34,35] and Cf[16,36] probably exhibit some sorts of site selectivity. Further theoretical works are highly desired.

Acknowledgements

This work was supported by the National Natural Science Foundation of China (Grant Nos. 22176181, 11874329, 11934020, and U1930121), the Foundation of the President of China Academy of Engineering Physics (Grant No. YZJJZQ2022011), and the Foundation of Science and Technology on Surface Physics and Chemistry Laboratory (Grant No. WDZC202101).

References

[1] Moore K T and van der Laan G 2009 *Rev. Mod. Phys.* **81** 235
[2] Zachariasen W H and Ellinger F H 1963 *Acta Crystall.* **16** 777
[3] Zachariasen W H and Ellinger F H 1963 *Acta Crystall.* **16** 369
[4] Lawson A C, Olsen C E, Richardson Jnr J W, Mueller M H and Lander G H 1988 *Acta Crystall. B* **44** 89
[5] Söderlind P, Eriksson O, Johansson B, Wills J M and Boring A M 1995 *Nature* **374** 524
[6] Zhu J X, Albers R C, Haule K, Kotliar G and Wills J M 2013 *Nat. Commun.* **4** 2644
[7] Kotliar G, Savrasov S Y, Haule K, Oudovenko V S, Parcollet O and Marianetti C A 2006 *Rev. Mod. Phys.* **78** 865
[8] Brito W H and Kotliar G 2019 *Phys. Rev. B* **99** 125113
[9] Amadon B 2016 *Phys. Rev. B* **94** 115148
[10] Qiu R, Ao B and Huang L 2020 *Comput. Mater. Sci.* **171** 109270
[11] Donohue J and Einspahr H 1971 *Acta Crystall. B* **27** 1740
[12] Li J, Ren Q, Lu C, Lu L, Dai Y and Liu B 2012 *J. Alloys Compd.* **516** 139
[13] Beeler B, Deo C, Baskes M and Okuniewski M 2013 *J. Nucl. Mater.* **433** 143
[14] Zhang H J, Li S N, Zheng J J, Li W D and Wang B T 2017 *Chin. Phys. B* **26** 066104
[15] Cococcioni M and de Gironcoli S 2005 *Phys. Rev. B* **71** 035105
[16] Huang L and Lu H 2019 *Phys. Rev. B* **99** 045109
[17] Huang L and Lu H 2020 *Phys. Rev. B* **101** 125123
[18] Liechtenstein A I, Anisimov V I and Zaanen J 1995 *Phys. Rev. B* **52** R5467
[19] Dudarev S L, Botton G A, Savrasov S Y, Humphreys C J and Sutton A P 1998 *Phys. Rev. B* **57** 1505
[20] Savrasov S Y and Kotliar G 2000 *Phys. Rev. Lett.* **84** 3670
[21] Shick A B, Drchal V and Havela L 2005 *Europhys. Lett.* **69** 588
[22] Shick A, Havela L, Kolorenč J, Drchal V, Gouder T and Oppeneer P M 2006 *Phys. Rev. B* **73** 104415
[23] Dorado B, Freyss M, Amadon B, Bertolus M, Jomard G and Garcia P 2013 *J. Phys.: Condens. Matter* **25** 333201
[24] Amadon B and Dorado B 2018 *J. Phys.: Condens. Matter* **30** 405603
[25] Kresse G and Furthmüller J 1996 *Phys. Rev. B* **54** 11169
[26] Ceperley D M and Alder B J 1980 *Phys. Rev. Lett.* **45** 566
[27] Perdew J P, Burke K and Ernzerhof M 1996 *Phys. Rev. Lett.* **77** 3865
[28] Blöchl P E 1994 *Phys. Rev. B* **50** 17953
[29] Kresse G and Joubert D 1999 *Phys. Rev. B* **59** 1758
[30] Meredig B, Thompson A, Hansen H A, Wolverton C and van de Walle A 2010 *Phys. Rev. B* **82** 195128
[31] Qiu R, Xie L and Huang L 2021 arXiv:2104.12440 [cond-mat.str-el]
[32] Villars P 1997 *Pearson's Handbook of Crystallographic Data for Intermediate Phases* (Cleveland: American Society of Metals)
[33] Roof R B, Haire R G, Schiferl D, Schwalbe L A, Kmetko E A and Smith J L 1980 *Science* **207** 1353
[34] Heathman S, Haire R G, Le Bihan T, Lindbaum A, Idiri M, Normile P, Li S, Ahuja R, Johansson B and Lander G H 2005 *Science* **309** 110
[35] Huang L, Chen R and Lu H 2020 *Phys. Rev. B* **101** 195123
[36] Heathman S, Le Bihan T, Yagoubi S, Johansson B and Ahuja R 2013 *Phys. Rev. B* **87** 214111